Analysis of laminated composites and sandwich structures by variable-kinematic MITC9 plate elements

Analysis of Laminated Composites and Sandwich Structures by Variable-Kinematic MITC9 plate elements

A. Pagani[1], S. Valvano[1], E. Carrera[1]

(1) Department of Mechanical and Aerospace Engineering,
Politecnico di Torino, Turin, Italy

Keywords:
Variable-Kinematic, Equivalent-Single-Layer, Layer-Wise, Finite Element Method, Carrera Unified Formulation, Plate.

Author and address for Correspondence
Dr. Alfonso Pagani
Research Assistant,
Department of Mechanical and Aerospace Engineering
Politecnico di Torino,
Corso Duca degli Abruzzi, 24,
10129 Torino, ITALY,
tel +39.011.546.6887, fax +39.011.564.6899
e.mail: alfonso.pagani@polito.it

Abstract

In this paper some advanced theories, obtained by expanding the unknown displacement variables along the thickness direction using Equivalent-Single-Layer (ESL) models, Layer-Wise (LW) models, and Variable-Kinematic models, are discussed. The used refined models are grouped in the Unified Formulation by Carrera (CUF), and they accurately describe the displacement field and the stress distributions along the thickness of the multilayered plate. The plate element has nine nodes, and the Mixed Interpolation of Tensorial Components (MITC) method is used to contrast the membrane and shear locking phenomenon. The governing equations are derived from the Principle of Virtual Displacement (PVD) and the Finite Element Method (FEM) is employed to solve them. Cross-ply plates with simply-supported edges and subjected to bi-sinusoidal load, multilayered cantilevered beams subjected to concentrate load and sandwich plates with simply-supported edges and subjected to costant transverse uniform pressure are analyzed. Various thickness ratios are considered. The results, obtained with different theories within CUF context, are compared with the elasticity solutions given in the literature. From the results it is possible to conclude that the plate element based on the CUF is very efficient in the study of composite structures. The Variable-Kinematic models combining the ESL with the LW models, permit to have a reduction of the computational costs, respect with the full LW models, preserving the accuracy of the results in localized layers.

1 Introduction

The continuous development of new structural materials, such as composite layered materials, leads to increasingly complex structural designs that require careful analysis. Plate/shell structures have a predominant role in a variety of engineering applications. The analysis of layered composite structures is complicated in practice. Anisotropy, nonlinear analysis as well as complicating effects, such as the C_z^0 - Requirements (zig-zag effects in the displacements and interlaminar continuity for the stresses), the couplings between in-plane and out-of-plane strains, are some of the issues to deal. In most of the practical problems, the solution demand applications of approximated computational methods. An overview on several computational techniques for the analysis of laminated structures can be read in the review articles [1, 2, 3].

The Finite Element Method (FEM) has a predominant role among the computational techniques implemented for the analysis of layered structures. The majority of FEM theories available in literature are formulated on the bases of axiomatic-type theories. The most-common used FEM theory is the classical Kirchhoff-Love theory and some examples are given in [4, 5]. Another classical plate/shell element is based on the First-order Shear Deformation Theory (FSDT), developed by Pryor and Barker [6], Noor [7], Hughes [8] and many others. A large variety of plate/shell finite element implementations of higher-order theories (HOT) have been proposed in the last twenty years literature. HOT-based C^0 finite elements (C^0 means that the continuity is required only for the unknown variables and not for their derivatives) were discussed by Kant and co-authors [9],[10]. Many other papers are available in which HOTs have been implemented for plates and shells, details can be found in the books by Reddy [11] and Palazotto and Dennis [12]. Dozens of finite elements have been proposed based on zig-zag theories [13, 14, 15, 16]. For multilayered structures, in literature, two kind of models can be adopted: the Equivlanet-Single-Layer (ESL) models, or the Layer-Wise (LW) models. The HOT type theories presented are ESL models, the variables are indipendent from the number of layers. Differently the LW models permit to consider different sets of variables per each layer. A finite element implementations of LW theories in the framework of axiomatic-type theories have been proposed by many authors, among which Noor and Burton [17], Reddy [18], Mawenya and Davies [19], Rammerstorfer et al. [20].

An improved plate finite element with a Variable-Kinematic model is here presented for the analysis

of composite structures. It is based on the Carrera's Unified Formulation (CUF), which was developed by Carrera for multi-layered structures [21, 22]. Both Equivalent Single Layer (ESL) and Layer Wise (LW) theories contained in the CUF have been implemented in the plate finite element. A Variable-Kinematic model obtained combining the ESL and LW models is developed. The Mixed Interpolation of Tensorial Components (MITC) method [23, 24, 25] is used to contrast the membrane and shear locking. The governing equations for the linear static analysis of composite structures are derived from the Principle of Virtual Displacement (PVD), in order to apply the finite element method. Cross-ply plates with simply-supported edges and subjected to bi-sinusoidal load, multilayered cantilevered beams with concentrated load and rectangular sandiwch plates with constant load are analyzed. The results, obtained with the different models contained in the CUF, are compared with the exact solution given in literature. This paper is organized as follows: geometrical and constitutive relations for plates are presented in Section 2. In Section 3, an overview of classical, higher-order and advanced plate theories developed within the CUF framework is given. Section 4 gives a brief outline of the FEM approach and the MITC9 method to overcome the problem of shear locking, whereas, in Section 5, the governing equations in weak form for the linear static analysis of composite structures are derived from the PVD. In Section 6 a short outline of the different modeling approaches is given, and the explanation of the Variable-Kinematic model is drawn. In Section 7, the results obtained using the proposed CUF theories are discussed. Section 8 is devoted to the conclusions.

2 Constitutive and geometrical relations for plates

Plates are bi-dimensional structures in which one dimension (in general the thickness in the z direction) is negligible with respect to the other two dimensions. The geometry and the reference system are indicated in Figure 1. The geometrical relations enable to express the in-plane $\boldsymbol{\epsilon}_p^k$ and out-plane $\boldsymbol{\epsilon}_n^k$ strains in terms of the displacement $\boldsymbol{u}$ for each layer k:

$$\boldsymbol{\epsilon}_p^k = [\epsilon_{xx}^k, \epsilon_{yy}^k, \epsilon_{xy}^k]^T = (\boldsymbol{D}_p^k)\ \boldsymbol{u}^k\ ,\ \boldsymbol{\epsilon}_n^k = [\epsilon_{xz}^k, \epsilon_{yz}^k, \epsilon_{zz}^k]^T = (\boldsymbol{D}_{np}^k + \boldsymbol{D}_{nz}^k)\ \boldsymbol{u}^k\ . \tag{1}$$

The explicit forms of the differential operators are:

$$\boldsymbol{D}_p^k = \begin{bmatrix} \partial_x & 0 & 0 \\ 0 & \partial_y & 0 \\ \partial_y & \partial_x & 0 \end{bmatrix}, \quad \boldsymbol{D}_{np}^k = \begin{bmatrix} 0 & 0 & \partial_x \\ 0 & 0 & \partial_y \\ 0 & 0 & 0 \end{bmatrix}, \quad \boldsymbol{D}_{nz}^k = \begin{bmatrix} \partial_z & 0 & 0 \\ 0 & \partial_z & 0 \\ 0 & 0 & \partial_z \end{bmatrix}, \tag{2}$$

The stress-strain relations are:

$$\begin{aligned} \boldsymbol{\sigma}_p^k &= \boldsymbol{C}_{pp}^k\ \boldsymbol{\epsilon}_p^k + \boldsymbol{C}_{pn}^k\ \boldsymbol{\epsilon}_n^k \\ \boldsymbol{\sigma}_n^k &= \boldsymbol{C}_{np}^k\ \boldsymbol{\epsilon}_p^k + \boldsymbol{C}_{nn}^k\ \boldsymbol{\epsilon}_n^k \end{aligned} \tag{3}$$

where

$$\begin{aligned} \boldsymbol{C}_{pp}^k &= \begin{bmatrix} C_{11}^k & C_{12}^k & C_{16}^k \\ C_{12}^k & C_{22}^k & C_{26}^k \\ C_{16}^k & C_{26}^k & C_{66}^k \end{bmatrix} \qquad \boldsymbol{C}_{pn}^k = \begin{bmatrix} 0 & 0 & C_{13}^k \\ 0 & 0 & C_{23}^k \\ 0 & 0 & C_{36}^k \end{bmatrix} \\ \boldsymbol{C}_{np}^k &= \begin{bmatrix} 0 & 0 & 0 \\ 0 & 0 & 0 \\ C_{13}^k & C_{23}^k & C_{36}^k \end{bmatrix} \qquad \boldsymbol{C}_{nn}^k = \begin{bmatrix} C_{55}^k & C_{45}^k & 0 \\ C_{45}^k & C_{44}^k & 0 \\ 0 & 0 & C_{33}^k \end{bmatrix} \end{aligned} \tag{4}$$

For the sake of brevity, the expressions that relate the material coefficients C_{ij} to the Young's moduli E_1, E_2, E_3, the shear moduli G_{12}, G_{13}, G_{23} and Poisson ratios ν_{12}, ν_{13}, ν_{23}, ν_{21}, ν_{31}, ν_{32} are not given here. They can be found in [18].

3 Carrera Unified Formulation for Plates

Classical plate models grant good results when thin thickness, homogeneous structures are considered. On the other hand, the analysis of thick plates, multilayered structures may require more sophisticated theories to achieve sufficiently accurate results. As a general guideline, it is clear that the richer the kinematic field, the more accurate the 2D model becomes. The CUF has the capability to expand each displacement variable at any desired order. Each variable can be treated independently from the others, according to the required accuracy. This procedure becomes extremely useful when multifield problems are investigated such as thermoelastic and piezoelectric applications [26, 27, 28, 29]. According to the CUF [22, 30, 31], the displacement field can be written as follows:

$$\begin{cases} u^k(x,y,z) = F_0(z)\, u_0^k(x,y) + F_1(z)\, u_1^k(x,y) + ... + F_N(z)\, u_N^k(x,y) \\ v^k(x,y,z) = F_0(z)\, v_0^k(x,y) + F_1(z)\, v_1^k(x,y) + ... + F_N(z)\, v_N^k(x,y) \\ w^k(x,y,z) = F_0(z)\, w_0^k(x,y) + F_1(z)\, w_1^k(x,y) + ... + F_N(z)\, w_N^k(x,y) \end{cases} \tag{5}$$

In compact form:

$$\boldsymbol{u}^k(x,y,z) = F_s(z)\boldsymbol{u}_s^k(x,y); \qquad \delta\boldsymbol{u}^k(x,y,z) = F_\tau(z)\delta\boldsymbol{u}_\tau^k(x,y) \qquad \tau, s = 0, 1, ..., N \tag{6}$$

where (x, y, z) is the general reference system (see Figure 1), and the displacement vector $\boldsymbol{u} = \{u, v, w\}$ has its components expressed in this system. $\delta\boldsymbol{u}$ is the virtual displacement associated to the virtual work and k identifies the layer. F_τ and F_s are the thickness functions depending only on z. $\boldsymbol{u}_s$ are the unknown variables depending on the coordinates x and y. τ and s are sum indexes and N is the number of terms of the expansion in the thickness direction assumed for the displacements. For the sake of clarity, the superscript k is omitted in the definition of the Taylor and Legendre polynomials.

3.1 Taylor Higher-order Theories

Classical plate models are based on Taylor polynomials. The Classical-Lamination-Theory (CLT) and the First-Shear-Deformation-Theory (FSDT) are based on a Taylor polynomial expansion including no more than costant and linear terms. Many attempts have been made to improve classical plate models. The Taylor polynomials express the unknown variables in function of the midplane position of the plate. This formulations are more efficient for thin, homogeneous structure than for thick, laminated plates. In this paper a Taylor higher-order polynomial expansion can be employed as thickness functions:

$$\boldsymbol{u} = F_0\, \boldsymbol{u}_0 + F_1\, \boldsymbol{u}_1 + \ldots + F_N\, \boldsymbol{u}_N = F_s\, \boldsymbol{u}_s, \qquad s = 0, 1, \ldots, N. \tag{7}$$

$$F_0 = z^0 = 1, \quad F_1 = z^1 = z, \quad \ldots, \quad F_N = z^N. \tag{8}$$

For Taylor polynomials, the letter N indicates the number of terms of the expansion and the polynomial order. For example, the theory $ET2$, an expansion of the second order, refers to the following displacement field:

$$\boldsymbol{u}(x,y,z) = \boldsymbol{u}_0(x,y) + z\, \boldsymbol{u}_1(x,y) + z^2\, \boldsymbol{u}_2(x,y) \tag{9}$$

Classical models, such as the CLT and FSDT, can be obtained as a particular case of an Equivalent-Single-Layer (ESL) theory with $N = 1$.

3.2 Legendre-like polynomial expansions

The limitations, due to expressing the unknown variables in function of the midplane position of the plate, can be overcome in several ways. A possible solution can be found employing the Legendre polynomials. They permit to express the unknown variables in function of the top and bottom position of a

part of the plate thickness. In the case of Legendre-like polynomial expansion models, the displacement is defined as follows:

$$\boldsymbol{u} = F_0\,\boldsymbol{u}_0 + F_1\,\boldsymbol{u}_1 + F_r\,\boldsymbol{u}_r = F_s\,\boldsymbol{u}_s, \qquad s = 0, 1, r\ , \quad r = 2, ..., N. \tag{10}$$

$$F_0 = \frac{P_0 + P_1}{2}, \quad F_1 = \frac{P_0 - P_1}{2}, \quad F_r = P_r - P_{r-2}. \tag{11}$$

in which $P_j = P_j(\zeta)$ is the Legendre polynomial of j-order defined in the ζ-domain: $-1 \leq \zeta \leq 1$. $P_0 = 1$, $P_1 = \zeta$, $P_2 = (3\zeta^2 - 1)/2$, $P_3 = (5\zeta^3 - 3\zeta)/2$, $P_4 = (35\zeta^4 - 30\zeta^2 + 3)/8$.
For the Layer-Wise (LW) models, the Legendre polynomials and the relative top and bottom position are defined for each layer.

4 Finite Element approximation and MITC9 method

Indipendently from the choice of the interpolating functions, a Finite Element approximation is employed and the MITC method is used to overcome the problem of the shear and membrane locking. In this section, the derivation of a plate finite element for the analysis of multilayered structures is presented. Considering a 9-node finite element, the displacement components are interpolated on the nodes of the element by means of the Lagrangian shape functions N_i, N_j:

$$\boldsymbol{u}_s = N_j \boldsymbol{u}_{s_j} \qquad \delta\boldsymbol{u}_\tau = N_i \delta\boldsymbol{u}_{\tau_i} \qquad \text{with} \quad i, j = 1, ..., 9 \tag{12}$$

where $\boldsymbol{u}_{s_j}$ and $\delta\boldsymbol{u}_{\tau_i}$ are the nodal displacements and their virtual variations. Therefore, equation (1) becomes:

$$\begin{aligned} \boldsymbol{\epsilon}_p &= F_s(\boldsymbol{D}_p)(N_j \boldsymbol{I})\boldsymbol{u}_{s_j} \\ \boldsymbol{\epsilon}_n &= F_s(\boldsymbol{D}_{np})(N_j \boldsymbol{I})\boldsymbol{u}_{s_j} + F_{s,_z}(N_j \boldsymbol{I})\boldsymbol{u}_{s_j} \end{aligned} \tag{13}$$

where $\boldsymbol{I}$ is the identity matrix. In classical FEM techniques, the strain components are computed from displacements by using geometrical relations (equation (13)). According to the MITC method ([32]-[33]) the strain components are reinterpolated employing a new set of Lagrangian shape function $\overline{N}$:

$$\begin{aligned} \overline{\boldsymbol{\epsilon}}_p &= \overline{N}_m \boldsymbol{\epsilon}_{p_m} \\ \overline{\boldsymbol{\epsilon}}_n &= \overline{N}_m \boldsymbol{\epsilon}_{n_m} \end{aligned} \tag{14}$$

where m indicates summation over the new set of points called *tying points*, the position of *tying points*, considering the local coordinate system (ξ, η), is different for each strain component. The new set of Lagrangian shape function $\overline{N}$ are defined in the *tying points*, for more details see [28]. The normal transverse strain ϵ_{zz} is excluded from this procedure, and it is directly calculated from the displacements.

5 Governing FEM equations

The PVD for a multilayered plate structure reads:

$$\int_{\Omega_k}\int_{A_k} \left\{ \delta\boldsymbol{\epsilon}_p^{k\,T}\boldsymbol{\sigma}_p^k + \delta\boldsymbol{\epsilon}_n^{k\,T}\boldsymbol{\sigma}_n^k \right\} d\Omega_k dz = \delta L_e \tag{15}$$

where Ω_k and A_k are the integration domains in the plane and the thickness direction, respectively. The left-hand side of the equation represents the variation of the internal work, while the right-hand side is the virtual variation of the external work. Substituting the constitutive equations (3), the geometrical relations written via the MITC method (14) and applying the CUF (6) and the FEM approximation (12), one obtains the following governing equations:

$$\delta \boldsymbol{q}^{k\tau i} : \quad \boldsymbol{K}^{k\tau sij} \boldsymbol{q}^{ksj} = \quad \boldsymbol{P}^{k\tau i} \tag{16}$$

where $\boldsymbol{K}^{k\tau sij}$ is a 3×3 matrix, called fundamental nucleus of the mechanical stiffness matrix, and its explicit expression is given in [34]. The nucleus is the basic element from which the stiffness matrix of the whole structure is computed. The fundamental nucleus is expanded on the indexes τ and s to obtain the stiffness matrix of each layer k. Then, the matrixes of each layer are assembled at the multi-layer level depending on the approach considered. $\boldsymbol{P}^{k\tau i}$ is a 3×1 matrix, called fundamental nucleus of the external load. $\boldsymbol{q}^{ksj}$ and $\delta \boldsymbol{q}^{k\tau i}$ are the nodal displacements and its variation respectively.

6 Modeling Approaches

Two different types of modeling approaches are usually used in literature:

- The Equivalent Single Layer models, here referred to as ESL
- The Layer Wise models, here referred to as LW

In this paper a third modeling approaches is taken into account. It is a variable kinematic model obtained as a combination of the ESL and LW models. The choice of the modeling approach is independent of the type of the used polynomials.

6.1 ESL models

In an ESL model, a homogenization of the properties of each layer is conducted by summing the contributions of each layer in the stiffness matrix. This process leads to a model that has a set of variables that is assumed for the whole multilayer. In this work the ESL model is employed using both Taylor and Legendre polynomials. The ESL assembly procedure of the stiffness matrix in the framework of CUF is shown in Figure 2.

6.2 LW models

LW considers different sets of variables per each layer, and the homogenization is just conducted at the interface level. The LW assembly procedure is presented in Figure 3. In this work the LW model is employed using the Legendre polymials. The Legendre polynomial F_0 and F_1 interpolate the displacements at the top (t) and bottom (b) position of the layer, respectively. The unknown variables at the top (t) and bottom (b) position are used to impose the following compatibility conditions:

$$\boldsymbol{u}_t^k = \boldsymbol{u}_b^{k+1}, \qquad k = 1, N_l - 1. \tag{17}$$

6.3 Variable-Kinematics

In this paper a different model is taken into account. This Variable-Kinematic model is obtained as a combination of the ESL and LW models. In order to combine these two different models the Legendre polynomials have been taken into account. In a multilayered structures some layers can be modeled with a homogenization of the properties and modeled with an ESL assembling procedure, whereas for some layers the homogenization is conducted just at the inferface level. This homogenization at the interface

level between the ESL and LW models is performed by the use of the Legendre polynomials. The Variable-Kinematic assembling, developed in the framework of the CUF, is very simple to integrate, for example in a FORTRAN code, with few lines of programming. The programming lines of the nucleus equations remain unchanged both for ESL, for LW and for Variable Kinematic assembling. The Variable-Kinematic assembly procedure of the stiffness matrix in the framework of CUF is shown in Figure 4.

Acronyms

Depending on the variables description and the number of terms N of the various expansion of kinematics plate theories can be obtained. A system of acronyms is given in order to denote these models. The first letters indicate the used approach in this work which is Equivalent Single Layer (E). The second letter indicate the type of polynomial adopted, (T) for the Taylor's polynomial expansion or (L) for the the Legendre's polynomials. Sometimes a reference solution is given with a layer-wise approach, so the first letters become LW. The number N indicates the number of terms of the expansion used in the thickness direction. If the Navier analytical method is employed the subscript (a) is used.

7 Numerical results

To assess these theories the following reference problems have been considered:

- A three-layer cross-ply square plate with lamination $(0°/90°/0°)$
- An eight-layer cantilevered beam
- A three-layer rectangular sandwich plate
- A five-layer composite sandwich plate

7.1 Three-layer composite plate

A three-layer cross-ply square plate, see Figure 1, with lamination $(0°/90°/0°)$ and simply-supported boundary condition is considered. The applied load is:

$$p\left(x, y, z_{top}\right) = \hat{p}\, sin\left(\frac{m\pi x}{a}\right) sin\left(\frac{n\pi y}{b}\right) \tag{18}$$

where $m = n = 1$. The mechanical properties of the material are: $E_L/E_T = 25$; $G_{LT}/E_T = 0,5$; $G_{TT}/E_T = 0,2$; $\nu_{LT} = \nu_{TT} = 0,25$. The geometrical dimensions are: $a = b = 1,0$. The mechanical load amplitude at the top position is: $\hat{p} = 1,0$. The results are presented for different thickness ratios $a/h = 4, 100$, and reported in non-dimensional form:

$$\hat{w} = \frac{100 w E_T h^3}{\hat{p}^+ a^4} \qquad ; \qquad \hat{\sigma}_{xx} = \frac{\sigma_{xx}}{\hat{p}^+ \left(\frac{a}{h}\right)^2} \qquad ; \qquad \hat{\sigma}_{xz/yz} = \frac{\sigma_{xz/yz}}{\hat{p}^+ \left(\frac{a}{h}\right)} \tag{19}$$

First a convergence study on the plate element was performed. A composite plate with thickness ratios $a/h = 100$, is evaluated. A mesh grid of 10×10 elements ensures the convergence, see Table 1. Therefore a locking study has been performed evaluating different types of integration methods [35] for the same plate structure to prove that the element is locking free, see Table 2. The plate element with the MITC9 method ensures accuracy on both the transverse displacement and the shear stress.
An assessment of the Legendre polynomials with a full ESL approach has been performed. All the results presented in Table 3, for thick and thin plates, show that the Legendre polynomials lead to the same results of the Taylor polynomials. Regarding the linear expansion $ET1$, if the thickness locking

correction is applied, $ET1^*$, a moderate difference in the results is noticeable, with respect $EL1$ theory. The use of either polynomials is invariant respect to the solution accuracy, see Figures 5-8.
Hereafter Legendre polynomials have been employed for the structure analyzes. Different Variable Kinematic models have been used to perform the analysis of the plate structures, see Figures 9-10. The acronyms have been modified adding a subscript to them, for the sake of clarity the list of subscripts is given below:

- $Case1 = \{layer1\}\,\{layer2, layer3\}$
- $Case2 = \{layer1, layer2\}\,\{layer3\}$

The results are listed in Table 4. For the plate structures analysed the following considerations can be drawn:

- Regarding the transverse displacement w the theories $EL4_{,Case1}$ and $EL4_{,Case2}$ lead a significant improvement of the solution respect to the $EL4$, see Figures 11,16.
- For the in-plane stress σ_{xx} the theories $EL4_{,Case1}$ and $EL4_{,Case2}$ improve the results in the interface zones, see Figure 12,17, with respect to the $EL4$.
- The transverse normal stress σ_{zz} does not show significant refinement of the solution, see Figure 13,18.
- For the shear stress σ_{xz} the results reach the exact solution in the layers that have a layer-wise assembling, the top layer for $EL4_{,Case1}$ and the bottom layer for $EL4_{,Case2}$, conversely the remaining layers with an equivalent-single-layer assembling have a loss of accuracy, see Figures 14-15,19-20.

7.2 Eight-layer composite beam

A cantilever eight-layer beam is analysed, see Figure 21. The structure is loaded at the free end with a concentrated load equal to $P_z = -0,2N$, applied at *top* position. The geometrical dimensions are: $a = 90\,mm$, $b = 1\,mm$, $h = 10\,mm$. The mechanical properties of the material labeled with the number 1 are: $E_L = 30\,GPa$, $E_T = 1\,GPa$, $G_{LT} = G_{TT} = 0,5\,GPa$, $\nu_{LT} = \nu_{TT} = 0,25$. Whereas the mechanical properties of the material labeled with the number 2 are: $E_L = 5\,GPa$, $E_T = 1\,GPa$, $G_{LT} = G_{TT} = 0,5\,GPa$, $\nu_{LT} = \nu_{TT} = 0,25$. The material stacking sequence is $[1/2/1/2]_s$. The FEM results of the present paper are compared with some solutions from the literature, and with the analytical solution derived by theory of elasticity presented in [36] and here called by the acronyms *Lekhnitskii*.
First of all, a convergence study on the plate element has been performed. A mesh grid of 12×2 elements ensures the convergence, see Table 5.
Different Variable Kinematic models have been used to perform the analysis of the plate structures. Depending on the combinations of the Variable Kinematic models, the acronyms have been modified adding a subscript to them to make the reading easier, for the sake of clarity the list of subscripts is given below:

- $Case1 = \{layer1\}\,\{layer2, layer3, layer4, layer5, layer6, layer7\}\,\{layer8\}$
- $Case2 = \{layer1, layer2\}\,\{layer3, layer4, layer5, layer6\}\,\{layer7, layer8\}$
- $Case3 = \{layer1\}\,\{layer2\}\,\{layer3, layer4, layer5, layer6\}\,\{layer7\}\,\{layer8\}$
- $Case4 = \{layer1, layer2, layer3\}\,\{layer4, layer5\}\,\{layer6, layer7, layer8\}$

The results are listed in Table 6. For the beam structure analysed the following considerations can be drawn:

- Regarding the transverse displacement w the theories $EL4_{,Case1}$, $EL4_{,Case2}$, $EL4_{,Case3}$ and $EL4_{,Case4}$ lead a significant improvement of the solution respect to the $EL4$, see Figure 22.
- For the in-plane stress σ_{xx} all the theories show the same accuracy, see Figure 23.
- For the transverse normal stress σ_{zz} the theories $EL4_{,Case1}$ and $EL4_{,Case3}$ lead a significant improvement of the solution respect to the $EL4$. The theories $EL4_{,Case2}$ and $EL4_{,Case4}$ show an improvement of the solution in the top layer of the beam, meanwhile a discontinuity of the σ_{zz} along the thickness is present, see Figure 24.
- For the shear stress σ_{xz} the $LW4$ solution reach the exact solution of the analytical reference solution (Lekhnitskii), see Figure 25(a). The results reach the exact solution in the layers that have a layer-wise assembling, the top and bottom layers for $EL4_{,Case1}$, see Figure 25(a), the first two top layers and last two bottom layers for $EL4_{,Case3}$, see Figure 25(c), the two central layers for $EL4_{,Case4}$, see Figure 25(d), conversely the remaining layers with an equivalent-single-layer assembling have a loss of accuracy, see Figures 25(a,b,c,d).

7.3 Three-layer sandwich plate

A 3 layered, unsymmetrically laminated, rectangular sandwich plate has been analyzed. The plate is simply-supported and loaded by a constant uniform pressure $P_z^{top} = -0.1\,MPa$ applied to the whole top surface. The geometrical dimensions are: $a = 100\,mm$, $b = 200\,mm$, $h = 12\,mm$. The faces have different thickness: $h_{top} = 0.1\,mm$, $h_{bottom} = 0.5\,mm$, and the core thickness is $h_{core} = 11.4\,mm$. The two faces have the following material data: $E_1 = 70000\,MPa$, $E_2 = 71000\,MPa$, $E_3 = 69000\,MPa$, $G_{12} = G_{13} = G_{23} = 26000\,MPa$, $\nu_{12} = \nu_{13} = \nu_{23} = 0.3$. The core made of metallic foam has the following data: $E_1 = E_2 = 3\,MPa$, $E_3 = 2.8\,MPa$, $G_{12} = G_{13} = G_{23} = 1\,MPa$, $\nu_{12} = \nu_{13} = \nu_{23} = 0.25$. The adopted mesh is the same of the three-layer composite plate, 10×10 elements.
Different Variable Kinematic models have been used to perform the analysis of the plate structures. The acronyms have been modified adding a subscript to them, for the sake of clarity the list of subscripts is given below:

- $Case1 = \{layer1\}\,\{layer2, layer3\}$
- $Case2 = \{layer1, layer2\}\,\{layer3\}$

The results of local values at top and bottom surfaces are listed in Table 7. It can be observed that although moderately thick plates are considered $a/h = (100/12)$, lower order theories as $ET1_a$, $EL1$, $EL2$, $EL1_{,Case1}$ and $EL1_{,Case2}$ lead to completely wrong results.
ESL models with Taylor or Legendre polynomials, also with higher order expansions, do not permit to obtain good results, $ET4$, $EL3$, $EL4$.
Variable-Kinematics models lead to some improvement starting from the second order of expansion, $EL2_{,Case1}$, $EL2_{,Case2}$, $EL3_{,Case1}$, etc. . For all the order of expansions of the Variable-Kinematics cases it has to be noted that the ($Case2$) cases have a better approximation of the results than the ($Case1$) cases, see Table 7. Very accurate models are required to capture the displacements and the stress distribution in the two faces.

7.4 Five-layer composite sandwich plate

A 5 layered composite sandwich plate has been analyzed. The plate is simply-supported and loaded by the same bi-sinusoidal load of the three-layer composite plate 7.1 applied to the whole top surface.

Different thickness ratios are considered, $a/h = 4, 100$. The thickness of the entire plate is fixed to $h = 0.01\,m$, so for thick plates $a = b = 0.04\,m$ and for thin plates $a = b = 1.0\,m$. The plates have four composite skins, two upper the core and tow lower the core. The thickness of the skins is $h_1 = h_2 = h_4 = h_5 = 0.0005\,m$. The ply sequence is $0°/90°/-90°/0°$. Their material properties are: $E_1 = 50\,GPa$, $E_2 = E_3 = 10\,MPa$, $G_{12} = G_{13} = G_{23} = 5\,GPa$, $\nu_{12} = \nu_{13} = \nu_{23} = 0.25$. The Nomex core has thickness $h_3 = 0.008\,m$. The core material properties are: $E_1 = E_2 = 0.01\,MPa$, $E_3 = 75.85\,MPa$, $G_{12} = G_{13} = G_{23} = 22.5\,MPa$, $\nu_{12} = \nu_{13} = \nu_{23} = 0.25$. The adopted mesh is the same of the three-layer composite plate, 10×10 elements.
Different Variable Kinematic models have been used to perform the analysis of the plate structures. The acronyms have been modified adding a subscript to them, for the sake of clarity the list of subscripts is given below:

- $Case1 = \{layer1\}\,\{layer2, layer3\}$
- $Case2 = \{layer1, layer2\}\,\{layer3\}$

The results are listed in Table 8.

8 Conclusions

This paper has dealt with the static analysis of composite and sandwich plates by means of a two-dimensional finite element based on the Unified Formulation. The element has been assessed by analyzing cross-ply plates under bi-sinusoidal loads and simply-supported boundary conditions, multilayered cantilevered beams under concentrated loads and sandwich plates under a costant transverse uniform pressure. The results have been presented in terms of both transverse displacement, in-plane stresses, transverse shear stresses, and transverse normal stress for various thickness ratios. The performances of the plate element have been tested, and the different theories (classical, refined, and Variable-Kinematic models) within the CUF framework have been compared. The following conclusions can be drawn:

1. The plate element with the MITC technique is locking free, for all the considered cases and for all the choosen models. The results converge to the reference solution by increasing the order of expansion of the displacements in the thickness direction, indipendently from the employed function type.

2. For multilayered composite plate, Variable-Kinematic models permit to improve the results with a reduction of computational costs, with respect to Layer-Wise solutions.

3. For multilayered structures the shear stresses can be modelized, in specific layers, by Variable-Kinematic models with the same accuracy of Layer-Wise theories, whereas strong reduction of computational costs can be obtained in the other layers.

4. For sandwich plate with weak core more accurate models are required. Employing Variable-Kinematic models it is possible to correctly take into account the discontinous behaviour of the sandwich layered structures.

References

[1] J N Reddy and D H Robbins. Theories and computational models for composite laminates. *Applied Mechanics Review*, 47:147–165, 1994.

[2] T K Varadan and K Bhaskar. Review of different theories for the analysis of composites. *Journal of Aerospace Society of India*, 49:202–208, 1997.

[3] E Carrera. Developments, ideas and evaluation based upon Reissner's Mixed Variational Theorem in the Modeling of Multilayered Plates and Shells. *Applied Mechanics Review*, 54:301–329, 2001.

[4] W T Koiter. On the foundations of the linear theory of thin elastic shell. *Proc. Kon. Nederl. Akad. Wetensch.*, 73:169–195, 1970.

[5] P G Ciarlet and L Gratie. Another approach to linear shell theory and a new proof of Korn's inequality on a surface. *C. R. Acad. Sci. Paris*, I,340:471–478, 2005.

[6] C W Pryor and R M Barker. A finite element analysis including transverse shear effect for applications to laminated plates. *American Institute of Aeronautics and Astronautics Journal*, 9:912–917, 1971.

[7] A K Noor. Finite element analysis of anisotropic plates. *American Institute of Aeronautics and Astronautics Journal*, 11:289–307, 1972.

[8] T J R Hughes and T Tezduyar. Finite elements based upon Mindlin plate theory with particular reference to the four-node isoparametric element. *Journal of Applied Mechanics*, 48:587–596, 1981.

[9] T Kant, D R J Owen, and O C Zienkiewicz. Refined higher order Cˆ0 plate bending element. *Computer & Structures*, 15:177–183, 1982.

[10] T Kant and J R Kommineni. Large amplitude free vibration analysis of cross-ply composite and sandwich laminates with a refined theory and Cˆ0 finite elements. *Computer & Structures*, 50:123–134, 1989.

[11] J N Reddy. Mechanics of laminated composite plates and shells. *Theory and Analysis, CRC Press*, 1997.

[12] A N Palazotto and S T Dennis. Nonlinear analysis of shell structures. *AIAA Series*, 1992.

[13] H Murakami. Laminated composite plate theory with improved in-plane responses. *Journal of Applied Mechanics*, 53:661–666, 1986.

[14] U Iscsro. Eight node zig-zag element for deflection and analysis of plate with general lay up. *Composites Part B*, pages 425–441, 1998.

[15] V R Aitharaju and R C Averill. Cˆ0 zig-zag kinematic displacement models for the analysis of laminated composites. *Mechanics of Composite Materials and Structures*, 6:31–56, 1999.

[16] Y B Cho and R C Averill. First order zig-zag sublaminate plate theory and finite element model for laminated composite and sandwich panels. *Computer & Structures*, 50:1–15, 2000.

[17] A K Noor and W S Burton. Assessment of computational models for multi-layered composite shells. *Applied Mechanics Review*, 43:67–97, 1990.

[18] J N Reddy. An evaluation of equivalent-single-layer and layerwise theories of composite laminates. *Composite Structures*, 25:21–35, 1993.

[19] A S Mawenya and J D Davies. Finite element bending analysis of multilayer plates. *Journal for Numerical Methods in Engineering*, 8:215–225, 1974.

[20] F G Rammerstorfer, K Dorninger, and A Starlinger. Composite and sandwich shells. *Nonlinear Analysis of Shells by Finite Elements*, 328:131–194, 1992.

[21] E Carrera. Theories and finite elements for multilayered, anisotropic, composite plates and shells. *Archives of Computational Methods in Engineering*, 9(2):87–140, 2002.

[22] E Carrera. Theories and finite elements for multilayered plates and shells: a unified compact formulation with numerical assessment and benchmarking. *Archives of Computational Methods in Engineering*, 10(3):215–296, 2003.

[23] K J Bathe, P S Lee, and J F Hiller. Towards improving the MITC9 shell element. *Computers and Structures*, 81:477–489, 2003.

[24] C Chinosi and L Della Croce. Mixed-interpolated elements for thin shell. *Communications in Numerical Methods in Engineering*, 14:1155–1170, 1998.

[25] N C Huang. Membrane locking and assumed strain shell elements. *Computers and Structures*, 27(5):671–677, 1987.

[26] E Carrera. An assessment of mixed and classical theories for the thermal stress analysis of orthotropic multilayered plates. *Journal of Thermal Stresses*, 23(9):797–831, 2000.

[27] M Cinefra, S Valvano, and E Carrera. Heat conduction and Thermal Stress Analysis of laminated composites by a variable kinematic MITC9 shell element. *Curved and Layered Structures*, 1:301–320, 2015.

[28] M Cinefra, E Carrera, and S Valvano. Variable Kinematic Shell Elements for the Analysis of Electro-Mechanical Problems. *Mechanics of Advanced Materials and Structures*, 22(1-2):77–106, 2015.

[29] M Cinefra, S Valvano, and E Carrera. A layer-wise MITC9 finite element for the free-vibration analysis of plates with piezo-patches. *International Journal of Smart and Nano Materials*, 6(2):85–104, 2015.

[30] E Carrera. Multilayered shell theories accounting for layerwise mixed description, Part 1: governing equations. *AIAA Journal*, 37(9):1107–1116, 1999.

[31] E Carrera. Multilayered shell theories accounting for layerwise mixed description, Part 2: numerical evaluations. *AIAA Journal*, 37(9):1117–1124, 1999.

[32] K J Bathe and E Dvorkin. A formulation of general shell elements - the use of mixed interpolation of tensorial components. *International Journal for Numerical Methods in Engineering*, 22:697–722, 1986.

[33] M L Bucalem and E Dvorkin. Higher-order MITC general shell elements. *International Journal for Numerical Methods in Engineering*, 36:3729–3754, 1993.

[34] M Cinefra and S Valvano. A variable kinematic doubly-curved MITC9 shell element for the analysis of laminated composites. *Mechanics of Advanced Materials and Structures, In Press.*

[35] T J R Hughes, M Cohen, and M Horaun. Reduced and selective integration techniques in the finite element methods. *Nuclear Engineering and Design*, 46:203–222, 1978.

[36] S G Lekhnitskii. Anisotropic Plates. In *Tsai, S W and Cheron, T editors (Translated from 2nd Russian Edition)*. Gordon & Branch, 1968.

[37] N J Pagano. Exact solutions for rectangular bidirectional composites and sandwich plate. *Journal of Composite Materials*, 4:20–34, 1970.

[38] M Petrolo, M Cinefra, A Lamberti, and E Carrera. Evaluation of Mixed Theories for Laminated Plates through the Axiomatic/Asymptotic Method. *Composites Part B*, 76:260–272, 2015.

[39] S H Nguyen and K S Surana. Two-dimensional curved beam element with higher-order hierarchical transverse approximation for laminated composites. *Computers & Structures*, 36:499–511, 1990.

[40] J F Davalos, Kim Y, and Barbero E J. Analysis of laminated beams with a layerwise constant shear theory. *Computers & Structures*, 28:241–253, 1994.

[41] Y Z Xiaoshan Lin. A novel one-dimensional two-node shear-flexible layered composite beam element. *Finite Elements in Analysis and Design*, 47:676–682, 2011.

[42] T P Vo and H T Thai. Static behavior of composite beams using various refined shear deformation theories. *Computers & Structures*, 94:2513–2522, 2012.

[43] E Carrera and A Ciuffreda. A unified formulation to asses theories of multilayered plates for various bending problems. *Composite Structures*, 69:271–293, 2005.

Tables

Table 1: Convergence study. Composite plate with lamination [0°/90°/0°] and with thickness ratio $a/h = 100$.

	Mesh	4×4	6×6	8×8	10×10
$LW4$	w	0.4349	0.4347	0.4347	0.4347
	σ_{xz}	0.415	0.404	0.400	0.398
$EL4$	w	0.4344	0.4343	0.4342	0.4342
	σ_{xz}	0.295	0.287	0.284	0.283
$ET4$	w	0.4344	0.4343	0.4342	0.4342
	σ_{xz}	0.295	0.287	0.284	0.282

Table 2: Locking study. Composite plate with lamination [0°/90°/0°] and with thickness ratio $a/h = 100$. All the cases are computed with a mesh of 10×10 elements.

		Reduced	*Selective*	$MITC9$	*Analytical*
$3D$[37]	w				-
	σ_{xz}				0.395
$LW4$	w	0.4347	0.4339	0.4347	0.4347
	σ_{xz}	0.616	0.664	0.398	0.395
$EL4$	w	0.4342	0.4334	0.4342	
	σ_{xz}	0.501	0.510	0.283	
$ET4$	w	0.4342	0.4334	0.4342	0.4342
	σ_{xz}	0.501	0.510	0.283	0.282

Table 3: Composite plate with lamination $[0°/90°/0°]$. Transverse displacement $\hat{w} = \hat{w}(a/2, b/2, +h/2)$, in-plane principal stress $\hat{\sigma}_{xx} = \hat{\sigma}_{xx}(a/2, b/2, \pm h/2)$, transverse shear stress $\hat{\sigma}_{xz} = \hat{\sigma}_{xz}(a, b/2, 0)$ and $\hat{\sigma}_{yz} = \hat{\sigma}_{yz}(a/2, b, 0)$. Taylor vs Legendre models.

	$a/h = 4$					$a/h = 100$					$DOFs$
	$\hat{w}$	$\hat{\sigma}_{xx}$		$\hat{\sigma}_{xz}$	$\hat{\sigma}_{yz}$	$\hat{w}$	$\hat{\sigma}_{xx}$		$\hat{\sigma}_{xz}$	$\hat{\sigma}_{yz}$	
		top	*bottom*				*top*	*bottom*			
$3D$[37]	-	0.801	-0.755	0.256	0.2172	-	0.539	-0.539	0.395	0.0828	
$LW4_a$ [38]	2.1216	0.801	-0.755	0.256	0.2180	0.4347	0.539	-0.539	0.395	0.0828	
$LW4$	2.1216	0.807	-0.761	0.258	0.2197	0.4347	0.544	-0.544	0.398	0.0836	17199
$ET4_a$ [38]	2.0083	0.786	-0.740	0.205	0.1830	0.4342	0.539	-0.539	0.281	0.0734	15
$ET4$	2.0082	0.7926	-0.7461	0.2067	0.1845	0.4342	0.5435	-0.5436	0.2830	0.0742	6615
$ET3$	2.0069	0.7940	-0.7479	0.2068	0.1845	0.4342	0.5436	-0.5436	0.2830	0.0742	5292
$ET2$	1.6499	0.4714	-0.4252	0.1219	0.1258	0.4333	0.5428	-0.5428	0.1436	0.0603	3969
$ET1^*$	1.6574	0.4484	-0.4537	0.1234	0.1237	0.4333	0.5428	-0.5428	0.1428	0.0592	2646
$ET1^-$	1.6448	0.4465	-0.4517	0.1227	0.1258	0.4282	0.5404	-0.5404	0.1421	0.0614	2646
$EL4$	2.0082	0.7926	-0.7461	0.2067	0.1845	0.4342	0.5435	-0.5436	0.2830	0.0742	6615
$EL3$	2.0069	0.7940	-0.7479	0.2068	0.1845	0.4342	0.5436	-0.5436	0.2830	0.0742	5292
$EL2$	1.6499	0.4714	-0.4252	0.1219	0.1258	0.4333	0.5428	-0.5428	0.1436	0.0603	3969
$EL1$	1.6448	0.4465	-0.4517	0.1227	0.1258	0.4282	0.5404	-0.5404	0.1421	0.0614	2646

$*$ *thickness locking correction*
$-$ *no correction*

Table 4: Composite plate with lamination $[0°/90°/0°]$. Transverse displacement $\hat{w} = \hat{w}(a/2, b/2, +h/2)$, in-plane principal stress $\hat{\sigma}_{xx} = \hat{\sigma}_{xx}(a/2, b/2, \pm h/2)$, transverse shear stress $\hat{\sigma}_{xz} = \hat{\sigma}_{xz}(a, b/2, 0)$ and $\hat{\sigma}_{yz} = \hat{\sigma}_{yz}(a/2, b, 0)$. Variable kinematic models.

	$a/h = 4$					$a/h = 100$					$DOFs$
	$\hat{w}$	$\hat{\sigma}_{xx}$		$\hat{\sigma}_{xz}$	$\hat{\sigma}_{yz}$	$\hat{w}$	$\hat{\sigma}_{xx}$		$\hat{\sigma}_{xz}$	$\hat{\sigma}_{yz}$	
		top	*bottom*				*top*	*bottom*			
$3D$[37]	-	0.801	-0.755	0.256	0.2172	-	0.539	-0.539	0.395	0.0828	
$LW4$	2.1216	0.807	-0.761	0.258	0.2197	0.4347	0.544	-0.544	0.398	0.0836	17199
$EL4_{,Case1}$	2.0865	0.7970	-0.7524	0.2548	0.1954	0.4346	0.5436	-0.5436	0.4006	0.0750	11907
$EL4_{,Case2}$	2.0862	0.7986	-0.7506	0.2530	0.1951	0.4346	0.5436	-0.5436	0.4006	0.0750	11907
$EL3_{,Case1}$	2.0803	0.7962	-0.7577	0.2395	0.1858	0.4345	0.5436	-0.5436	0.3568	0.0727	9261
$EL3_{,Case2}$	2.0818	0.8034	-0.7500	0.2398	0.1889	0.4345	0.5436	-0.5436	0.3568	0.0727	9261
$EL2_{,Case1}$	2.0671	0.7851	-0.7431	0.2378	0.1750	0.4345	0.5436	-0.5436	0.3569	0.0679	6615
$EL2_{,Case2}$	2.0675	0.7901	-0.7394	0.2380	0.1759	0.4345	0.5436	-0.5436	0.3569	0.0679	6615
$EL1_{,Case1}$	1.7328	0.6288	-0.3581	0.1480	0.1386	0.4317	0.5425	-0.5430	0.1795	0.0635	3969
$EL1_{,Case2}$	1.6925	0.3774	-0.5854	0.1411	0.1339	0.4317	0.5430	-0.5425	0.1795	0.0635	3969
$EL4$	2.0082	0.7926	-0.7461	0.2067	0.1845	0.4342	0.5435	-0.5436	0.2830	0.0742	6615
$EL3$	2.0069	0.7940	-0.7479	0.2068	0.1845	0.4342	0.5436	-0.5436	0.2830	0.0742	5292
$EL2$	1.6499	0.4714	-0.4252	0.1219	0.1258	0.4333	0.5428	-0.5428	0.1436	0.0603	3969
$EL1$	1.6448	0.4465	-0.4517	0.1227	0.1258	0.4282	0.5404	-0.5404	0.1421	0.0614	2646

Table 5: Convergence study. Eight-layer cantilever beam. Transverse displacement $w = -10^2 w(a, b/2, 0)$, in-plane principal stress $\sigma_{xx} = 10^3 \sigma_{xx}(a/2, b/2, +h/2)$, transverse shear stress $\sigma_{xz} = 10^2 \sigma_{xz}(a/2, b/2, 0)$.

	Mesh	2×2	4×2	6×2	8×2	10×2	12×2
$LW4$	w	3.031	3.032	3.031	3.030	3.030	3.030
	σ_{xx}	651	690	716	725	728	730
	σ_{xz}	2.991	2.797	2.792	2.791	2.790	2.789
$EL4$	w	3.029	3.029	3.029	3.028	3.028	3.028
	σ_{xx}	684	723	730	731	731	731
	σ_{xz}	3.054	2.829	2.821	2.822	2.822	2.822

Table 6: Eight-layer cantilever beam. Transverse displacement $w = w(a, b/2, 0)$, in-plane principal stress $\sigma_{xx} = \sigma_{xx}(a/2, b/2, +h/2)$, transverse shear stress $\sigma_{xz} = \sigma_{xz}(a/2, b/2, 0)$.

	$-w \times 10^2\,(mm)$	$\sigma_{xx} \times 10^3\,(MPa)$	$\sigma_{xz} \times 10^2\,(MPa)$	$DOFs$
Nguyen and Surana [39]	3.031	720		
Davalos et al. [40]	3.029	700		
Xiaoshan [41]	3.060	750		
Vo and Thai [42]	3.024			
Lekhnitskii [36]		730	2.789	
$LW4$	3.030	730	2.789	12375
$EL4_{,Case1}$	3.029	730	2.773	4875
$EL4_{,Case2}$	3.029	731	2.854	4875
$EL4_{,Case3}$	3.030	730	2.854	7875
$EL4_{,Case4}$	3.029	731	2.788	4875
$EL3_{,Case1}$	3.029	731	2.773	3750
$EL3_{,Case2}$	3.029	731	2.854	3750
$EL3_{,Case3}$	3.030	731	2.854	6000
$EL3_{,Case4}$	3.028	731	2.788	3750
$EL2_{,Case1}$	3.021	731	2.360	2625
$EL2_{,Case2}$	3.025	731	2.593	2625
$EL2_{,Case3}$	3.027	731	2.593	4125
$EL2_{,Case4}$	3.026	731	2.775	2625
$EL1_{,Case1}$	3.017	730	2.357	1500
$EL1_{,Case2}$	3.012	731	2.592	1500
$EL1_{,Case3}$	3.023	730	2.592	2250
$EL1_{,Case4}$	2.996	731	2.774	1500
$EL4$	3.028	731	2.822	1875
$EL3$	3.027	731	2.822	1500
$EL2$	2.980	731	2.005	1125
$EL1$	2.981	729	2.000	750

Table 7: Sandwich rectangular plate. Transverse displacement $w = w(a/2, b/2, \pm h/2)$, in-plane principal stresses $\sigma_{xx} = \sigma_{xx}(a/2, b/2)$ and $\sigma_{yy} = \sigma_{yy}(a/2, b/2)$.

	w		σ_{xx}				σ_{yy}				$DOFs$
	top	*bottom*	Top Skin		Bottom Skin		Top Skin		Bottom Skin		
			top	*bottom*	*top*	*bottom*	*top*	*bottom*	*top*	*bottom*	
$LW4_a$[43]	-9.142	-8.968	-112.4	-48.435	-133.21	166.27	-52.824	-23.320	-54.327	69.915	
$LW4$	-9.140	-8.968	-110.7	-51.073	-132.85	166.10	-50.519	-25.617	-53.664	69.254	17199
$ET1_a$[43]	-0.1022	-0.1020	-89.63	-88.715	15.508	20.008	-51.453	-50.932	8.4375	11.041	
$ET4$	-6.138	-6.031	-83.621	-81.922	-84.422	114.60	-28.265	-50.032	-35.270	46.817	6615
$EL4_{,Case1}$	-7.0933	-6.9667	-103.84	-57.814	-100.44	131.90	-47.740	-28.419	-41.748	54.605	11907
$EL4_{,Case2}$	-8.1492	-7.9967	-88.077	-78.083	-115.99	149.22	-28.613	-49.735	-46.729	62.324	11907
$EL3_{,Case1}$	-5.6061	-5.5118	-98.957	-62.599	-77.967	112.48	-45.764	-30.385	-33.885	49.155	9261
$EL3_{,Case2}$	-8.0258	-7.8758	-97.903	-69.009	-113.98	147.20	-38.471	-40.344	-45.904	61.499	9261
$EL2_{,Case1}$	-4.7261	-4.6580	-97.159	-66.531	-86.447	123.39	-45.014	-31.995	-51.271	68.389	6615
$EL2_{,Case2}$	-6.9117	-6.7812	-109.20	-61.634	-96.204	129.19	-51.057	-30.000	-38.608	54.121	6615
$EL1_{,Case1}$	-0.1271	-0.1255	-88.364	-87.142	14.684	20.341	-40.693	-40.007	5.8738	9.0807	3969
$EL1_{,Case2}$	-0.1570	-0.1631	-88.379	-87.267	13.850	21.281	-40.930	-40.298	6.0253	10.149	3969
$EL4$	-6.1381	-6.0307	-83.621	-81.922	-84.422	114.60	-28.265	-50.032	-35.270	46.817	6615
$EL3$	-1.4379	-1.4206	-90.232	-82.528	-17.848	54.888	-42.125	-39.696	-14.416	31.674	5292
$EL2$	-0.1264	-0.1286	-88.361	-87.534	15.110	19.996	-41.420	-41.038	6.7722	9.0627	3969
$EL1$	-0.1022	-0.1019	-90.065	-89.146	15.589	20.182	-51.489	-50.967	8.4427	11.048	2646

Table 8: Composite sandwich plate. Transverse displacement $\hat{w} = \hat{w}(a/2, b/2, +h/2)$, in-plane principal stress $\hat{\sigma}_{xx} = \hat{\sigma}_{xx}(a/2, b/2, \pm h/2)$, transverse shear stress $\hat{\sigma}_{xz} = \hat{\sigma}_{xz}(a, b/2, 0)$ and $\hat{\sigma}_{zz} = \hat{\sigma}_{zz}(a/2, b/2, +h/2)$. Variable kinematic models.

	$a/h = 4$					$a/h = 100$					$DOFs$
	$\hat{w}$	$\hat{\sigma}_{xx}$		$\hat{\sigma}_{xz}$	$\hat{\sigma}_{zz}$	$\hat{w}$	$\hat{\sigma}_{xx}$		$\hat{\sigma}_{xz}$	$\hat{\sigma}_{zz}$	
		top	$bottom$				top	$bottom$			
$LW4$	-	-	-	-	-	-	-	-	-	-	-
$EL4_{,Case1}$	-	-	-	-	-	-	-	-	-	-	-
$EL4_{,Case2}$	-	-	-	-	-	-	-	-	-	-	-
$EL3_{,Case1}$	-	-	-	-	-	-	-	-	-	-	-
$EL3_{,Case2}$	-	-	-	-	-	-	-	-	-	-	-
$EL2_{,Case1}$	-	-	-	-	-	-	-	-	-	-	-
$EL2_{,Case2}$	-	-	-	-	-	-	-	-	-	-	-
$EL1_{,Case1}$	-	-	-	-	-	-	-	-	-	-	-
$EL1_{,Case2}$	-	-	-	-	-	-	-	-	-	-	-
$EL4$	-	-	-	-	-	-	-	-	-	-	-
$EL3$	-	-	-	-	-	-	-	-	-	-	-
$EL2$	-	-	-	-	-	-	-	-	-	-	-
$EL1$	-	-	-	-	-	-	-	-	-	-	-

Figures

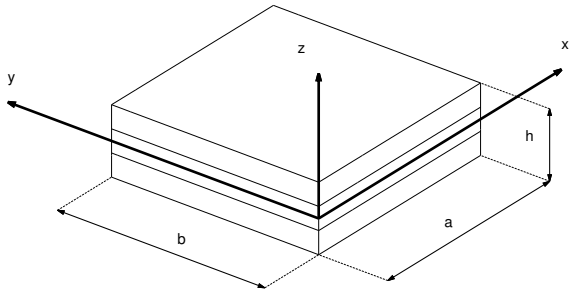

Figure 1: Reference system of the plate.

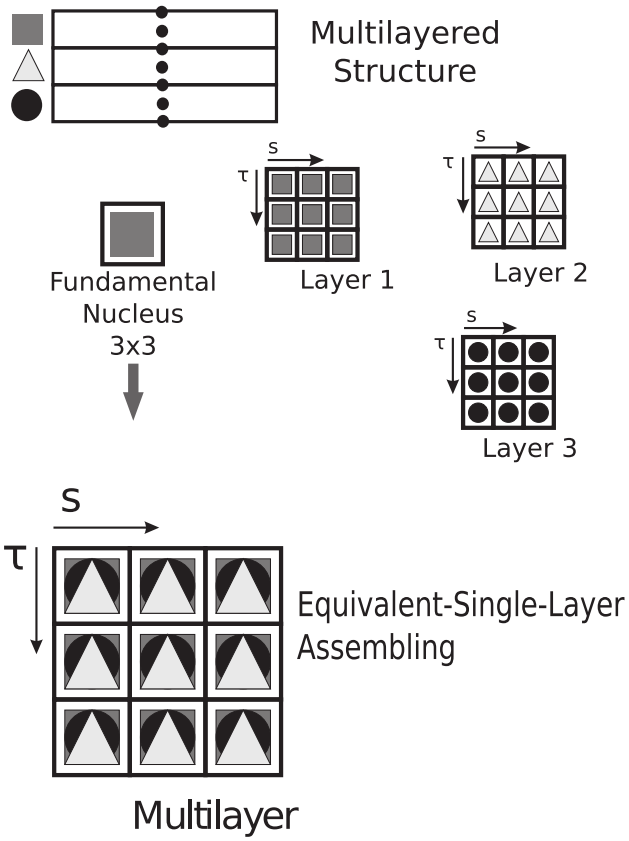

Figure 2: Equivalent-Single-Layer assembling scheme.

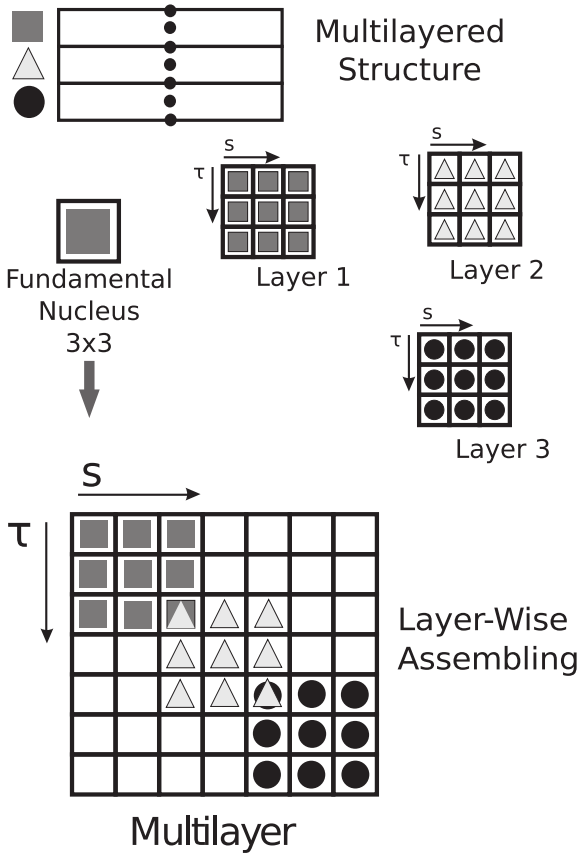

Figure 3: Layer-Wise assembling scheme.

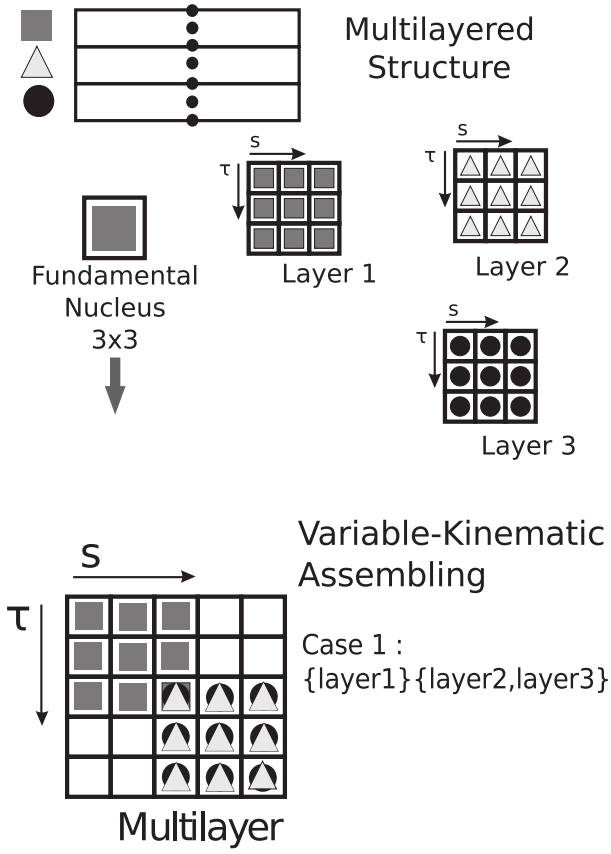

Figure 4: Variable-Kinematic assembling scheme.

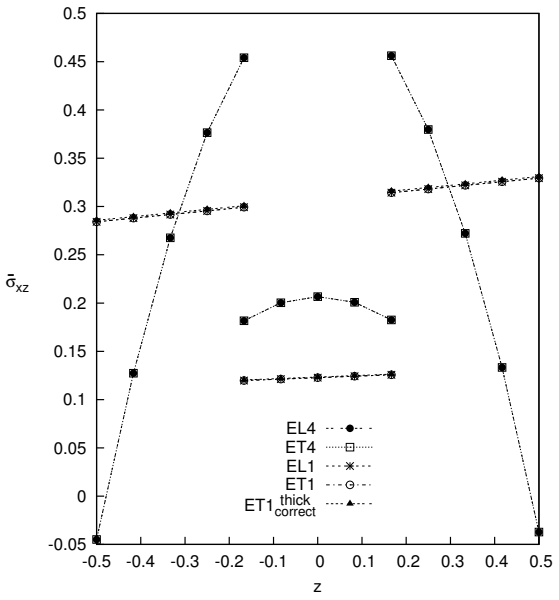

Figure 5: Transverse shear stress $\boldsymbol{\sigma}_{xz}$ along the thickness, with thickness ratio $(a/h) = 4$. Composite plate.

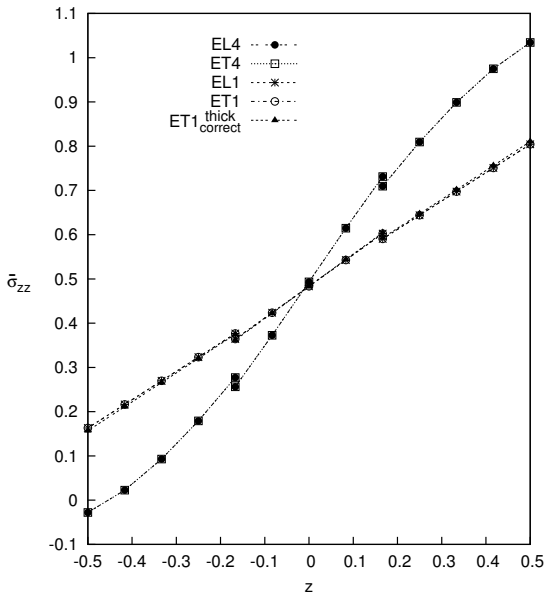

Figure 6: Transverse normal stress $\boldsymbol{\sigma}_{zz}$ along the thickness, with thickness ratio $(a/h) = 4$. Composite plate.

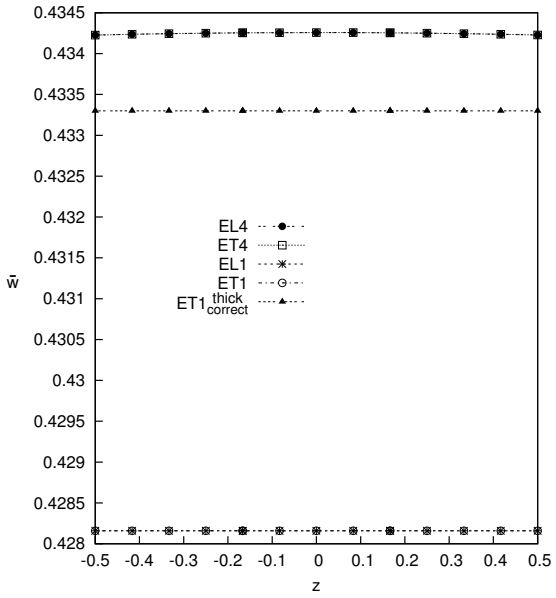

Figure 7: Transverse displacement $\boldsymbol{w}$ along the thickness, with thickness ratio $(a/h) = 100$. Composite plate.

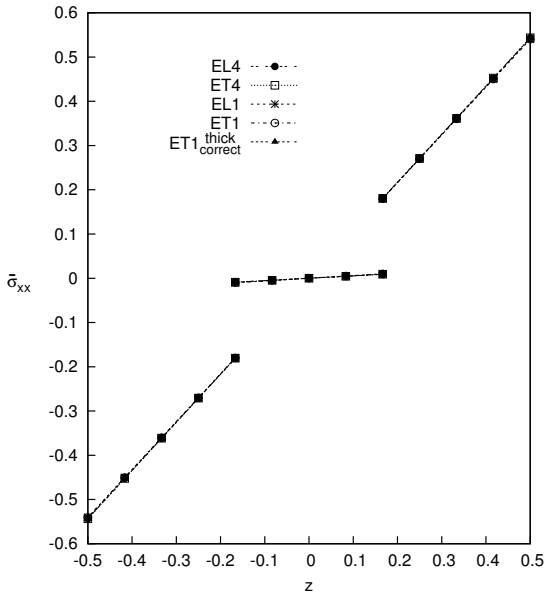

Figure 8: In-plane stress $\boldsymbol{\sigma}_{xx}$ along the thickness, with thickness ratio $(a/h) = 100$. Composite plate.

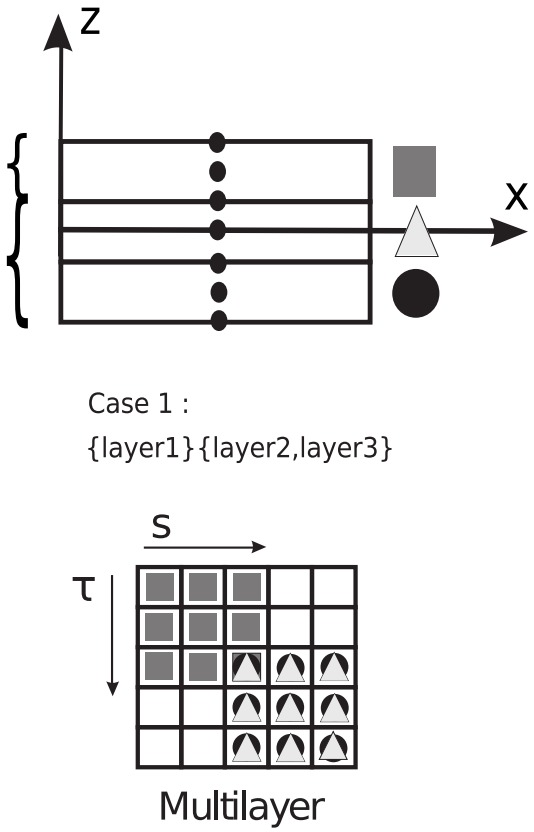

Figure 9: Variable Kinematic Model for the three-layer plate. Case 1.

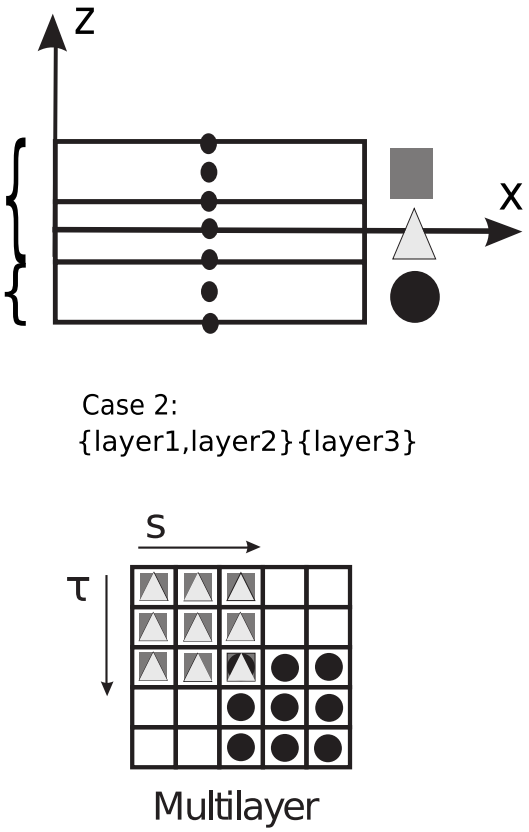

Figure 10: Variable Kinematic Model for the three-layer plate. Case 2.

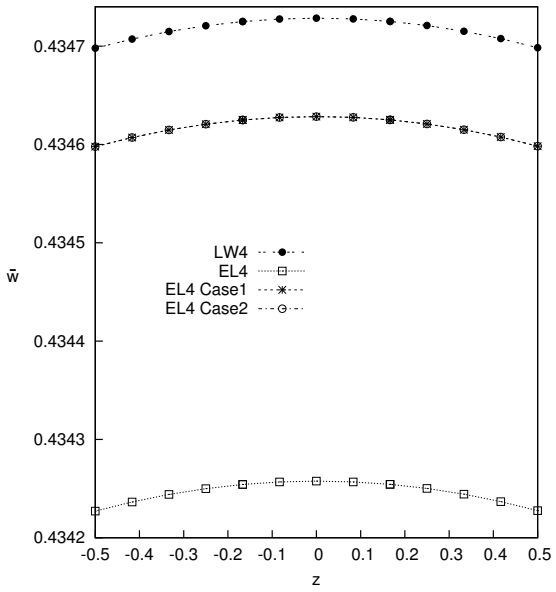

Figure 11: Transverse displacement $\boldsymbol{w}$ along the thickness, with thickness ratio $(\,a\,/\,h\,) = 100$. Composite plate.

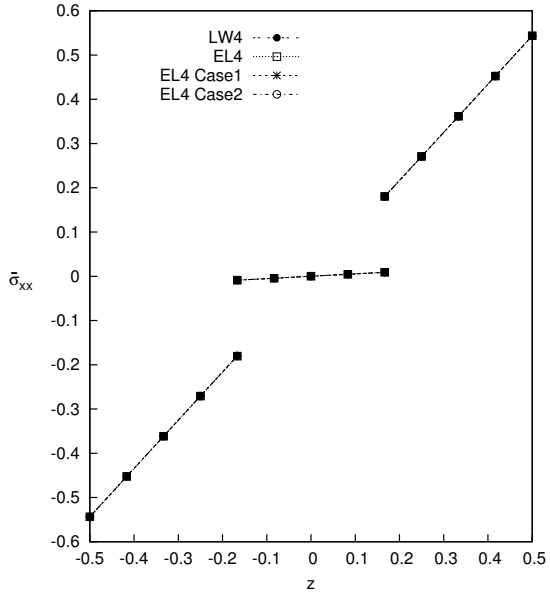

Figure 12: In-plane stress $\boldsymbol{\sigma}_{xx}$ along the thickness, with thickness ratio $(\,a\,/\,h\,) = 100$. Composite plate.

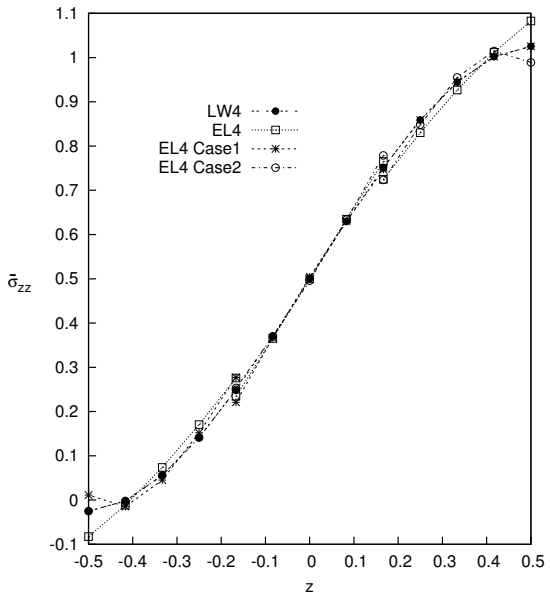

Figure 13: Transverse normal stress $\boldsymbol{\sigma}_{zz}$ along the thickness, with thickness ratio $(\,a\,/\,h\,) = 100$. Composite plate.

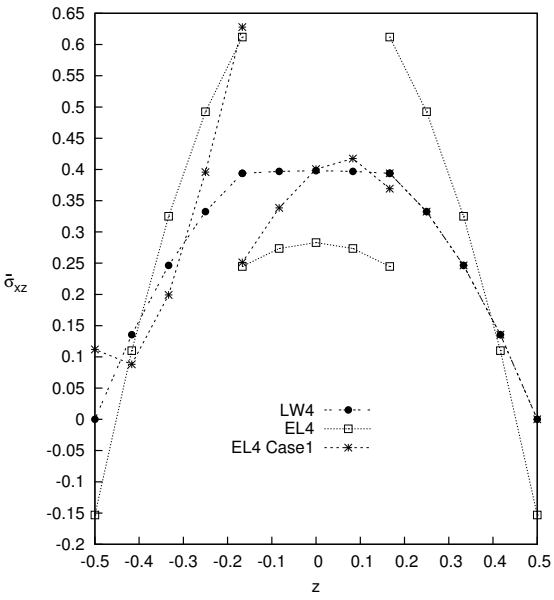

Figure 14: Transverse shear stress $\boldsymbol{\sigma}_{xz}$ along the thickness, with thickness ratio $(\,a\,/\,h\,) = 100$. Composite plate.

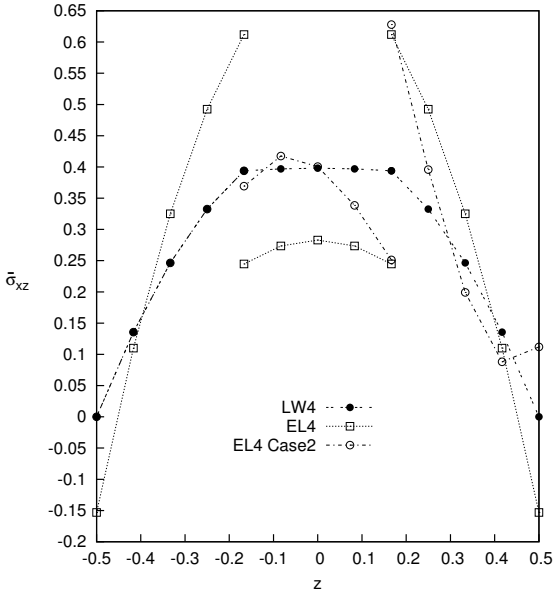

Figure 15: Transverse shear stress $\boldsymbol{\sigma}_{xz}$ along the thickness, with thickness ratio $(\,a\,/\,h\,) = 100$. Composite plate.

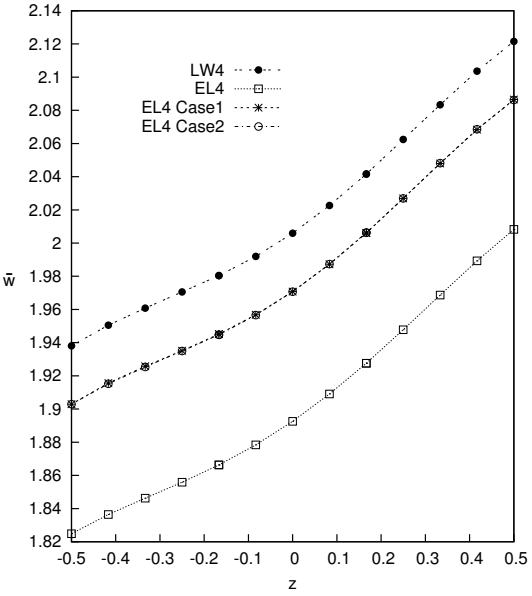

Figure 16: Transverse displacement $\boldsymbol{w}$ along the thickness, with thickness ratio $(\,a\,/\,h\,) = 4$. Composite plate.

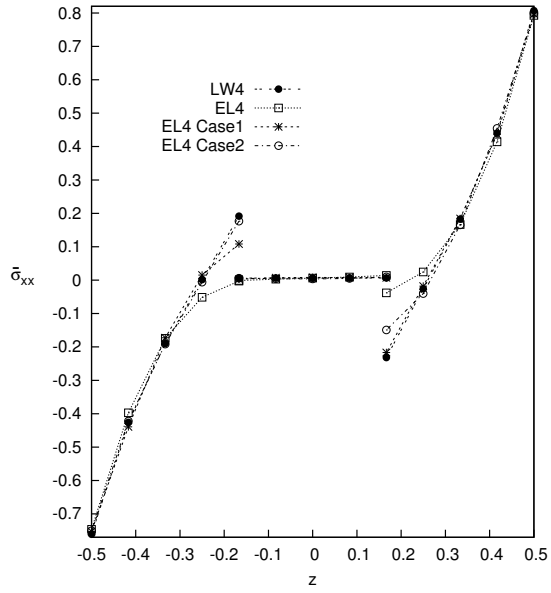

Figure 17: In-plane stress $\boldsymbol{\sigma}_{xx}$ along the thickness, with thickness ratio $(\,a\,/\,h\,) = 4$. Composite plate.

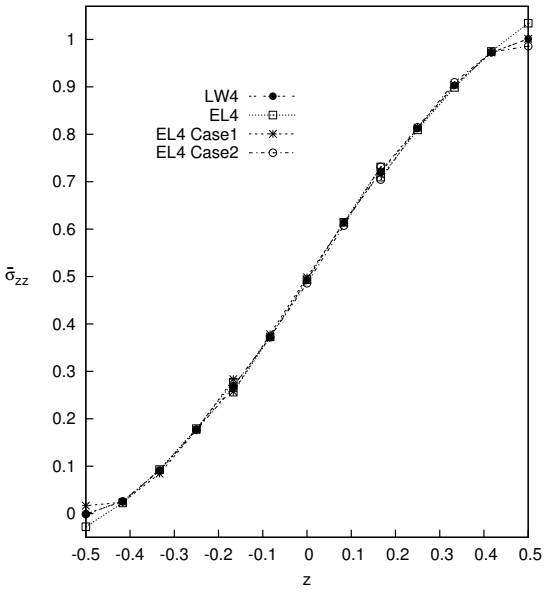

Figure 18: Transverse normal stress $\boldsymbol{\sigma}_{zz}$ along the thickness, with thickness ratio $(\,a\,/\,h\,) = 4$. Composite plate.

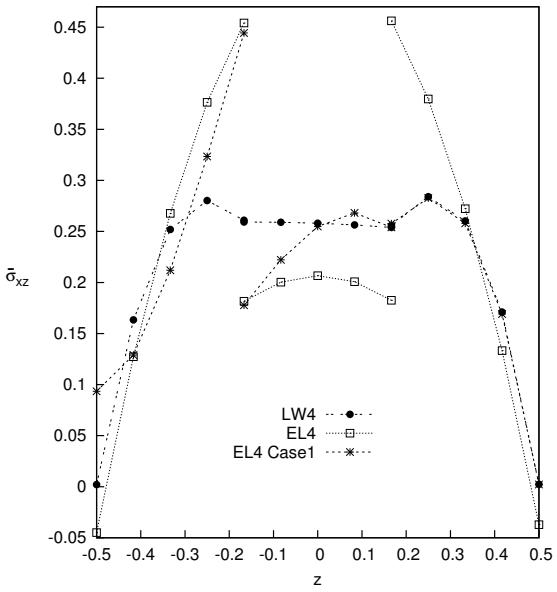

Figure 19: Transverse shear stress $\boldsymbol{\sigma}_{xz}$ along the thickness, with thickness ratio $(\,a\,/\,h\,) = 4$. Composite plate.

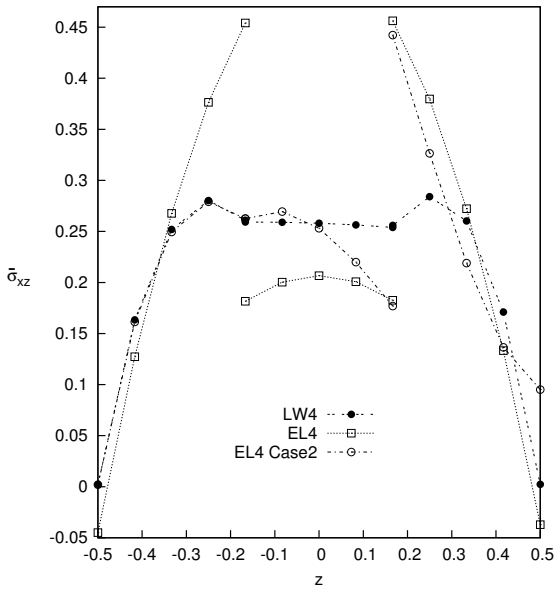

Figure 20: Transverse shear stress $\boldsymbol{\sigma}_{xz}$ along the thickness, with thickness ratio $(\,a\,/\,h\,) = 4$. Composite plate.

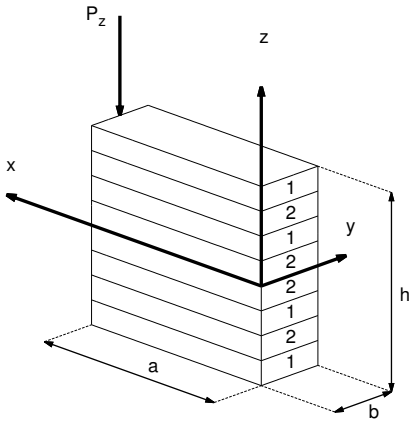

Figure 21: Reference system of the eight-layer beam with a concentrated load. The material lamination scheme is indicated with label 1 and label 2.

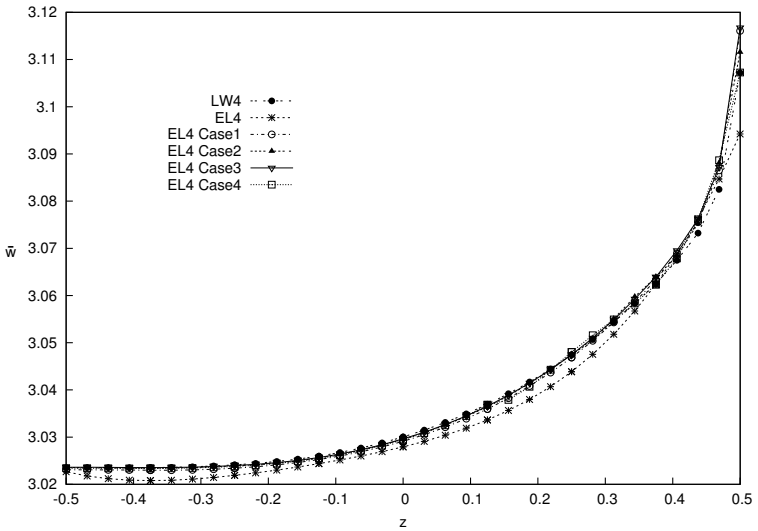

Figure 22: Transverse displacement $\boldsymbol{w}$ along the thickness, with thickness ratio $(\,L\,/\,h\,) = 9$. Composite beam.

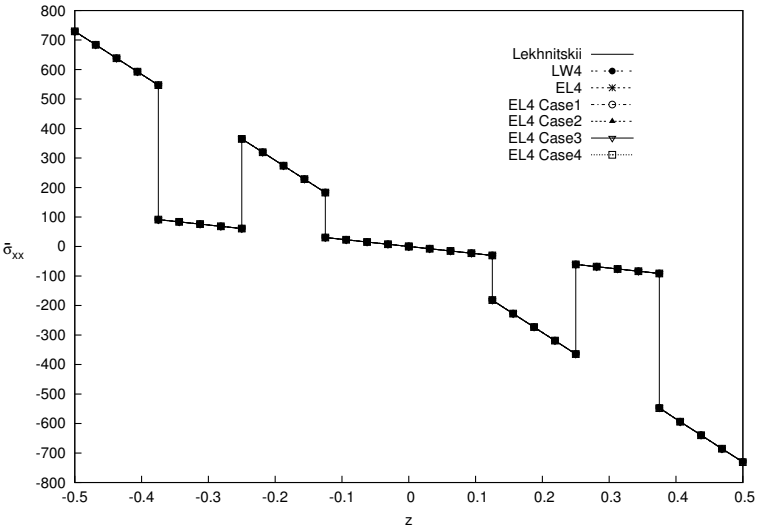

Figure 23: In-plane stress $\boldsymbol{\sigma}_{xx}$ along the thickness, with thickness ratio $(L/h) = 9$. Composite beam.

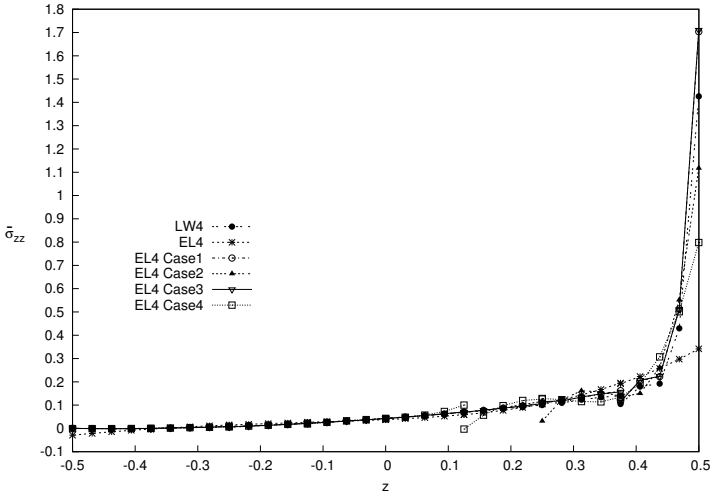

Figure 24: Transverse normal stress $\boldsymbol{\sigma}_{zz}$ along the thickness, with thickness ratio $(L/h) = 9$. Composite beam.

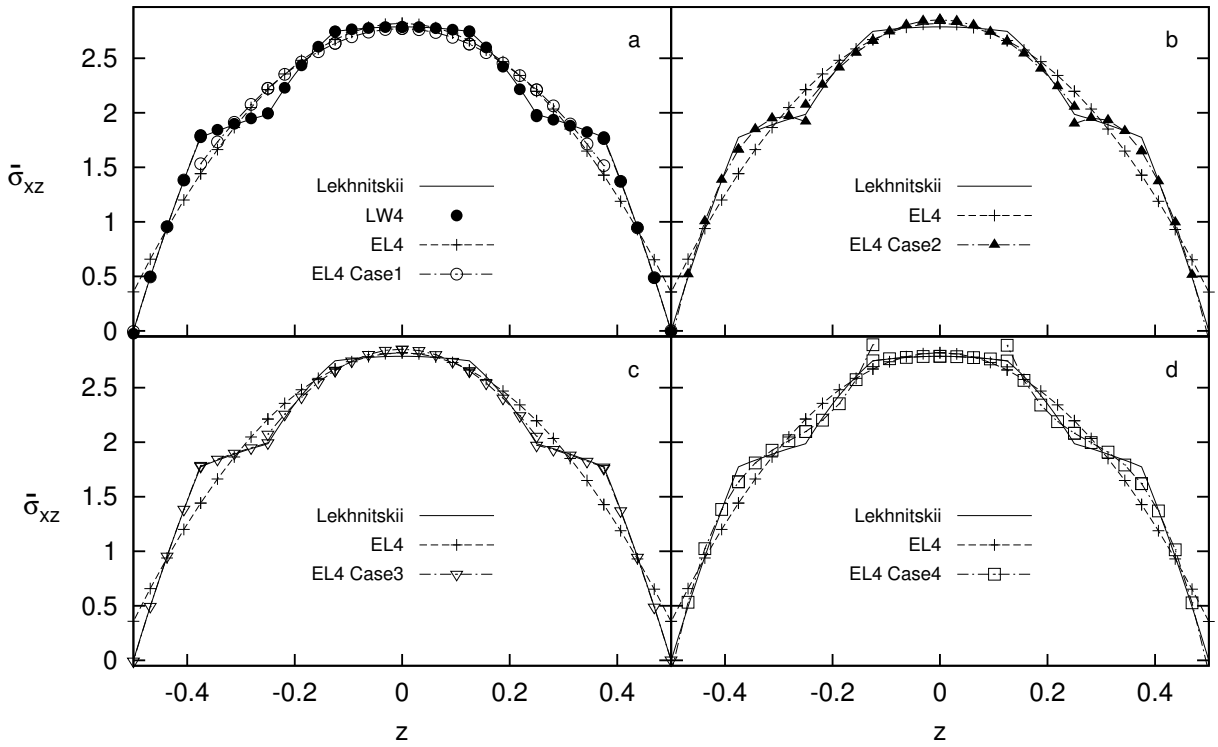

Figure 25: Transverse shear stress $\boldsymbol{\sigma}_{xz}$ along the thickness, with thickness ratio $(L/h) = 9$. Composite beam.